Biosensors and Bioelectronics 274 (2025) 117152

Contents lists available at ScienceDirect

Biosensors and Bioelectronics

journal homepage: www.elsevier.com/locate/bios

An aptamer-based electrochemical sensor for the quantification of the malaria biomarker lactate dehydrogenase

Qiuyue Yang [a,**], Julia Pedreira-Rincón [a,b], Leire Balerdi-Sarasola [a,c], Luis Baptista-Pires [d,e], Jose Muñoz [a,b,c], Daniel Camprubí-Ferrer [a,c], Andrea Idili [f], Claudio Parolo [a,g,*]

[a] Barcelona Institute for Global Health (ISGlobal), Barcelona, 08036, Spain
[b] Facultat de Medicina i Ciències de la Salut, Universitatde Barcelona (UB), Barcelona, 08036, Spain
[c] International Health Department, Hospital Clínic de Barcelona,Barcelona, 08036, Spain
[d] I3N, Physics Department, University of Aveiro, Aveiro, 3810-193, Portugal
[e] Graphenicalab: Parc Científic Tecnocampus, Mataró, 08302, Spain
[f] Department of Chemical Sciences and Technologies, University of Rome Tor Vergata, Via della Ricerca Scientifica, Rome 00133, Italy
[g] INTERFIBIO Research Group, Departament d'Enginyeria Química, Universitat Rovira i Virgili, Tarragona, 43007, Spain

ARTICLE INFO

Keywords:
Electrochemical aptamer-based sensor
Malaria diagnosis
Point-of-care device
Whole blood

ABSTRACT

Malaria is one of the most deadly infectious diseases, causing the death of hundreds of thousands of patients each year. Global efforts to combat malaria necessitate the implementation of novel rapid diagnostic tests deployable at the point of care. Here, we present the development of an electrochemical aptamer-based (EAB) sensor for the quantification of the malaria biomarker Plasmodium falciparum lactate dehydrogenase (PfLDH). Specifically, we demonstrate how, through careful optical and electrochemical characterization, we re-engineered the aptamer sequence to maximize its binding-induced conformational change, the core principle of EAB sensors. We then demonstrated that our biosensor can quantify clinically relevant concentrations of PfLDH in blood in a single step and within a few minutes. Overall, we believe these results demonstrate the promising potential of EAB sensors for the diagnosis and prognosis of malaria at the point of care.

1. Introduction

Malaria is the most widespread parasitic disease and is considered one of the three most deadly infectious diseases, along with HIV and tuberculosis, due to its high mortality rate and widespread prevalence (Bourzac, 2014). In 2022 alone, malaria was responsible for over 600, 000 deaths, primarily affecting children, pregnant women, and adults from regions where malaria is not endemic. World malaria report (2023, 2023) Given its relevance in public health, it is no surprise that malaria has been a major target for several public and private initiatives aimed at its control and elimination, including the Malaria Eradication Scientific Alliance (MESA) hosted by our institute (Home - MESA, 2011). Thanks to these actions, in recent years, we have observed a decrease in the number of malaria cases and, hopefully, with the upcoming vaccines, we may see even further improvements (Malaria vaccine: WHO position paper, 2024). Despite the tremendous efforts the global community is making to cure and prevent malaria, it remains one of the deadliest diseases worldwide. In this context, the World Health Organization (WHO) has indicated that the development of reliable point-of-care (PoC) diagnostic tests is crucial in our fight against malaria, not only to aid clinical decisions but also as tools to assess epidemiological interventions (Global Tecnichal Strategy for Malaria, 2021).

Currently, the gold standard methods to diagnose malaria are microscopic techniques and molecular tests based on polymerase chain reaction (PCR) (Fig. 1A). Ballard et al. (2019) Despite these methods provide sensitive and specific results, they cannot support mass-screening tests. Both methods require specialized personnel and dedicated equipment resulting in cumbersome, time-consuming, and costly diagnostic processes. On the contrary, given their low cost and ease of use (Parolo et al., 2020a), lateral flow assays (LFA) have become the most widely used diagnostic devices for diagnosing malaria in malaria-endemic, low- and middle-income countries (Global malaria programme, 2023). Remarkably, commercially available LFAs have achieved clinical sensitivities and specificities in malaria diagnostics of

* Corresponding author. Barcelona Institute for Global Health (ISGlobal) Hospital Clınic - Universitat de Barcelona, Barcelona, 08036, Spain.
** Corresponding author.
E-mail addresses: qiuyue.yang@isglobal.org (Q. Yang), claudio.parolo@isglobal.org (C. Parolo).

https://doi.org/10.1016/j.bios.2025.117152
Received 12 October 2024; Received in revised form 23 December 2024; Accepted 9 January 2025
Available online 16 January 2025

over 95% (Bell and Visser, 2016). However, their analytical performances have recently been compromised by the deletion of the histidine-rich protein-2 (HRP2) antigen, which led to an increase in the number of false-negative results (Poti et al., 2020). To tackle this problem, some commercial LFAs now incorporate two analytes (i.e., HRP2 and lactate dehydrogenase (LDH)). Despite the strong impact that LFAs have in malaria diagnostics, their qualitative naked-eye readout has two main limitations (Lynch et al., 2022). On one hand, the result is inevitably subjective to the end user, making the assessment of faint lines challenging. On the other hand, although it has been suggested that parasite biomarkers could be associated with disease severity, the lack of quantitative measurement prevents their use as potential prognostic devices; that is, they cannot be employed to identify severe from non-severe patients, a crucial aspect for prioritizing the use of limited healthcare resources (Hendriksen et al., 2012). Therefore, the development of novel sensing platforms and biosensors capable of providing rapid, quantitative, and quantitative results is essential to address the limitations of current diagnostic tools and enable more efficient and effective malaria control and management strategies.

Establishing the quantitative measurement of clinically relevant biomarkers at the point-of-care is crucial to shifting clinical practice from the "one-size-fits-all" to the "personalized medicine" paradigm (Fig. 1B) (Balanza et al., 2020; Balerdi-Sarasola et al., 2023). A clear example of how quantitative measurements can change treatment and improve the quality of life of a patient is the glucometer, which, by enabling precise and timely management of blood sugar levels, helps reduce diabetes-related complications (Van Enter and Von Hauff, 2018). Unfortunately, this approach cannot be easily employed for every class of targets, as the success of the glucometer lies in the use of the highly sensitive and specific enzyme glucose oxidase (Parolo et al., 2023). To tackle this problem, we and others have been working on a new class of biosensors called electrochemical aptamer-based (EAB) sensors (Fig. 1B, bottom) a sensing technology that employs aptamers as recognition element (Parolo et al., 2023). In EAB sensors, their signal transduction mechanism depends on the binding-induced conformational change of the aptamer itself. Specifically, the aptamer is anchored at one end on the electrode surface and modified at the other end with a redox reporter (here methylene blue (MB)). In the presence of the target, the aptamer undergoes a conformational change which, in turn, affects the relative position of the redox probe from the electrode surface (Fig. 1B, bottom). This change affects the efficiency of the redox probe to exchange electrons with the surface generating a measurable electrochemical signal whose intensity is related to the target concentration (Fig. 1B, bottom). Arroyo-Currás et al. (2020) Thanks to this mechanism, EAB sensors allow the rapid measurement (within 15 min typically) (Curtis et al., 2019) of a wide variety of target analytes (Arroyo-Currás et al., 2017; Idili et al., 2021; Parolo et al., 2020b) directly in untreated biological fluids (without any washing or incubation steps) in vivo and in vitro (Arroyo-Currás et al., 2020), making them perfect candidate for diagnostic applications at the point-of-care.

Given the limitations of current malaria diagnostic methods, we sought to develop an EAB sensor for rapid, point-of-care malaria

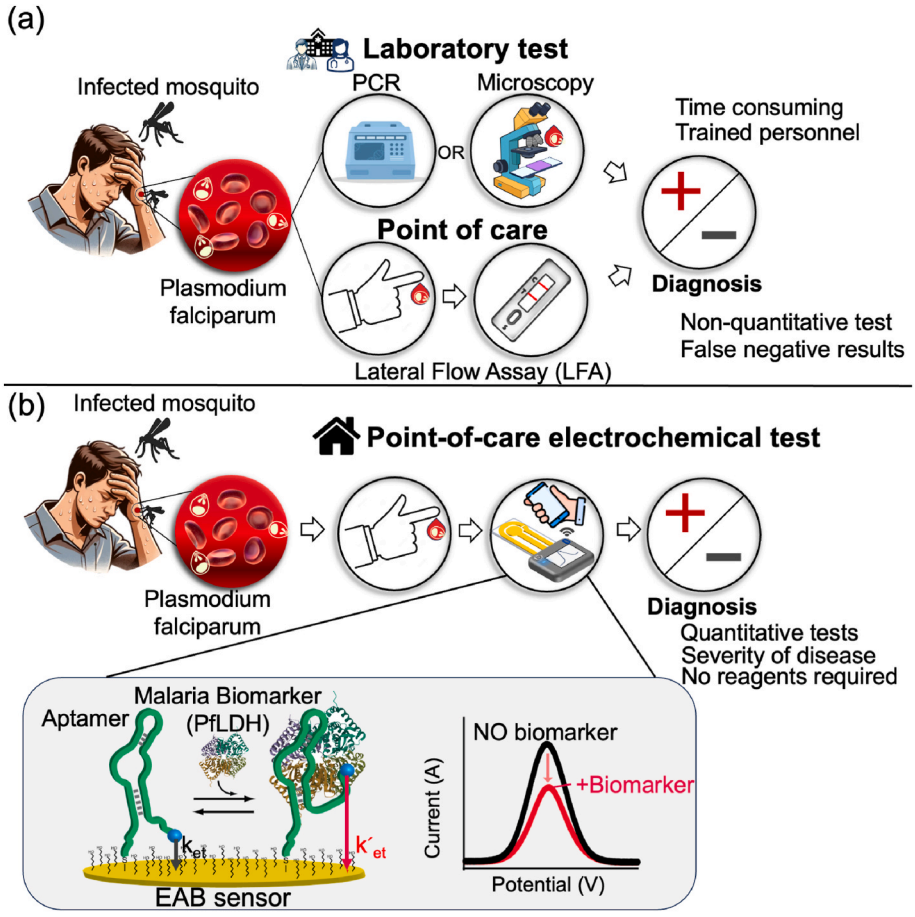

Fig. 1. (A) Current malaria diagnostic methods are labor-intensive and require specialized expertise, hindering effective patient monitoring and treatment optimization in developed countries. In addition, lateral flow assays allow for point of care diagnosis of the disease, but their naked-eye reading results in no quantitative measurements and in end-user error. (B) The development of a rapid, point-of-care diagnostic test for malaria would significantly improve patient management by enabling timely and personalized treatment decisions. Specifically, EAB sensors will enable the single step measurement of PfLDH in diluted blood, allowing for the prompt diagnosis and potentially prognosis of malaria.

detection to improve disease management and control in endemic regions (Fig. 1B). Here we present the development of a novel EAB sensor for the measurement of *P. falciparum* lactate dehydrogenase (PfLDH). Firstly, we describe the re-engineering process of the native aptamer sequence. Through a rational design of the sequences we generate variants able to undergo the required binding-induced conformational change. Then, we used optical techniques to characterize the new aptamer variants and select the candidates showing the larger conformational change in the presence of the target (i.e., higher signal gain). Finally, we adapted the re-engineered aptamer variants to support the electrochemical platform. We demonstrate their ability to generate responsive EAB sensors able to detect clinically relevant concentrations of PfLDH (Plucinski et al., 2019) directly in diluted human blood (two-steps).

2. Experimental section

2.1. Materials and Methods

Chemical reagents are reagent-grade, including phosphate buffered saline tablets (PBS), sodium hydroxide (NaOH), sulfuric acid 96% (H_2SO_4), 6-mercapto-1-hexanol, sodium chloride (NaCl), ethanol (CH_3CH_2OH), magnesium chloride ($MgCl_2$), and tris(2-carboxyethyl)-phosphine hydrochloride (TCEP) which were obtained from Sigma-Aldrich (St. Louis, MO, USA). A polishing kit (including the 1-μm monocrystalline diamond slurry, the 0.04-μm gamma Alumina slurry and micro-cloths) was acquired from Schmitz-Metallographie GmbH, Aachen Germany. The oligos including 1) 5′modified with 6-Fam and 3′modified by BMN, and 2) 5′modified with HO-C6-S-S- and 3′ with AttoMB2 were purchased from Biomers GmbH (Ulm, Germany). Protein targets including the recombinant PfLDH (34.9 kDa), HRP2 (63 kDa) and Native Human CRP (114 kDa) were obtained from Sino Biological Europe GmbH (Eschborn, Germany), Abcam (Cambridge, UK) and Bio-Rad Laboratories (Hercules, CA, USA), respectively. Healthy human blood was purchased from Hospital Clinic Barcelona. The whole electrochemical station, including the CHI1030C potentiations, the gold disk electrodes (CHI101 with diameter of 3 mm), fritted Ag|AgCl electrodes in 1M KCl (CHI111 reference electrode) and platinum wire (CHI115 counter electrode) were purchased from CHInstruments Inc (Austin, TX, USA). Water to prepare solutions of proteins and buffers is deionized with resistance greater than 18.2 MΩ cm^{-1}.

2.2. Fluorescence measurements

In order to optically asses the binding-induced conformational change of the different aptamer variants (named P11-46, P11-40, P11-35, P11-30 and 40-P11, 2008–35, 2008–30, 2008–25, 2008–20) we purchased the corresponding DNA sequences modified at their 5′ end with a fluorophore (6-fam) and at their 3′ end with a quencher (BMN-Q535). Using a black 384-microwell plate, we mixed 80 μL of each optical probe (depending on the experiment at a concentration of 10, 30 or 100 nM in PBS) with 15 μL of either PBS or PfLDH at the concentrations required for each particular experiments (i.e., between 300 pM and 3 μM). The plate was read using the TECAN 200 pro Mnano, employing an excitation wavelength of 475 nm and recording an emission wavelength of 520 nm (gain 100; # flashes 25; integration time 20 μs; Z position 20000 μm). The time constant (τ) is obtained based on the fitting results of fluorescent intensity vs time in the kinetic measurement, with the equation of the first-order exponential decay:

$$y = Ae^{\frac{-t}{\tau}} + y_0$$

The normalizad signal change is calculated:

$$normalized\ signal\ change = \frac{(FL(concentration) - FL(0))}{FL(0)}$$

FL(0) is the fluorescent intensity without any addition with PfLDH, measured at the same time with FL(conconcentration).

2.3. Electrochemical test

Cleaning: The working electrodes were polished with diamond and alumina slurries on a piece of microcloth, repeating drawing an eight-pattern for 3 min in each step. Afterwards, the electrodes were sonicated in a mixed solution of ethanol and water (v:v = 1:1) using a bath sonicator for 5 min (two times) at room temperature. Then, they were further electrochemically cleaned as previously reported (Xiao et al., 2007) by performing successive scans in 0.5 M NaOH, 0.5 M sulfuric acid, and a mixture of 0.1 M sulfuric acid with 0.01 M KCl.

Immobilization: In parallel of cleaning electrodes, 4 μL of thiol- and methylene-blue-modified aptamers (100 μM) were reduced by adding 8 μL of TCEP solution (10 mM) and incubating for 1.5 h. Before immobilizing onto the electrode surface, the reduced aptamer solutions were diluted by adding 788 μL of an assembling buffer (consisting of 10 mM phosphate with 1.0 M NaCl and 1 mM Mg^{2+}, pH = 7.2–7.4) to reach a final concentration of 500 nM. Afterwards, the electrodes were incubated with the aptamers for 1.5 h in the dark, cleaned with water, dried by nitrogen gas, and then transferred to a 6-mercaptohexanol solution (20 mM in assembling buffer) overnight at 4 °C in the fridge.

Stabilization before use: We cleaned the electrodes with water in the following day, and stored them in PBS solution in fridge. All the electrodes were tested within this day. Before testing, the electrodes were stabilized in PBS by running square wave voltammetries using a potential range from −0.46 V to −0.12 V, the potential step of 0.001 V, and amplitude of 0.025 V with different frequencies.

DATA analysis: The peak height was obtained through CHInstrument software using the linear baseline subtraction tool. All the fittings were done using the software Origin 2018.

$$signal\ change = \frac{(Ip(concentration) - Ip(\text{baseline}))}{Ip(\text{baseline})}$$

Ip(baseline) is the peak intensity without any addition of PfLDH, followed by the measurement of Ip (concentration).

Fitting data with 4 parameter logistic curve:

$$y = Start + (Start - End)\frac{x^n}{x^n + Kd^n}$$

where y represents the response variable, which is fluorescent intensity, or electrochemical signal change. x is the concentration of PfLDH in the assay. Kd is the dissociation constant. n is the Hill coefficient. Start is the fitted baseline response at the lowest concentration, while End is the fitted saturation response to the highest concentration.

3. Results and discussion

3.1. Design of the aptamer receptor

As recognition element for our sensor we identified two potential aptamers specific for PfLDH: one called “2008s” selected by Prof. Tanner’s group (Cheung et al., 2013) and the other called “P11” selected by Prof. Limson’s group (Table S1) (Frith et al., 2018). We selected these aptamers because they exhibit nanomolar binding activity and have been adapted to optical and electrochemical sensing platforms (Cheung et al., 2013; Figueroa-Miranda et al., 2018, 2020; Frith et al., 2018; Minopoli et al., 2020). The former is 35 bases long, while the latter is 46 bases long and both display GC-rich stem-loop structures. The aptamer sequences have been selected using classical SELEX which ensures that the aptamers have high binding activity for the selected target, but no a structure-switching behavior (Cheung et al., 2013; Frith et al., 2018). Consequently, we re-engineered the aptamer sequences to undergo a conformational change integrating a signal-tradition mechanism

regulated by the binding of the target. To do this, we rationally design variants of the parent sequences by shortening them from the 5′ or 3′ ends in increments of approximately 5 bases (Fig. 1A and S1). Our goal is to destabilize the native structure to populate a more unfolded conformation and induce a large-scale conformational change in the presence of the target (Shaver et al., 2022). To rationally design the variants we used the nucleic acid folding predictor NUPACK (NUPACK-Cloudalpha, 2006) to estimate their folding thermodynamics and obtain a structural prediction of their conformation. We designed 10 truncated aptamer variants, 4 for the 2008 (Fig. S1) and 6 for the P11 sequences (Fig. 2A). Specifically, for the three truncates of 2008 aptamer (2008–30, 2008–25, and 2008–20), we observe a decrease in the stability of the aptamer from the −4.8 kcal/mol of the parent sequence to as low as −1.8 kcal/mol for 2008–20 (Fig. S2). This is followed by the reorganization of the native conformation resulting in different stem-loop structures (Fig. S2). We observe the same thing for the P11 aptamer. The three truncated variants (P11-40, P11-35, and P11-30) show lower stabilities from the −5.0 kcal/mol of the parent sequence to as low as −0.9 kcal/mol for P11-30 (Fig. S3). Again, the structures for this set of variants are different from the parent aptamer. In contrast, for the two truncates from the 5′ end (40-P11 and 35-P11) there is a small change in stability and their conformations are similar to the parent aptamer (Fig. S3).

3.2. Optical characterization

To characterize the ability of the re-engineered aptamer variants to undergo a binding-induced conformational change, we labeled them

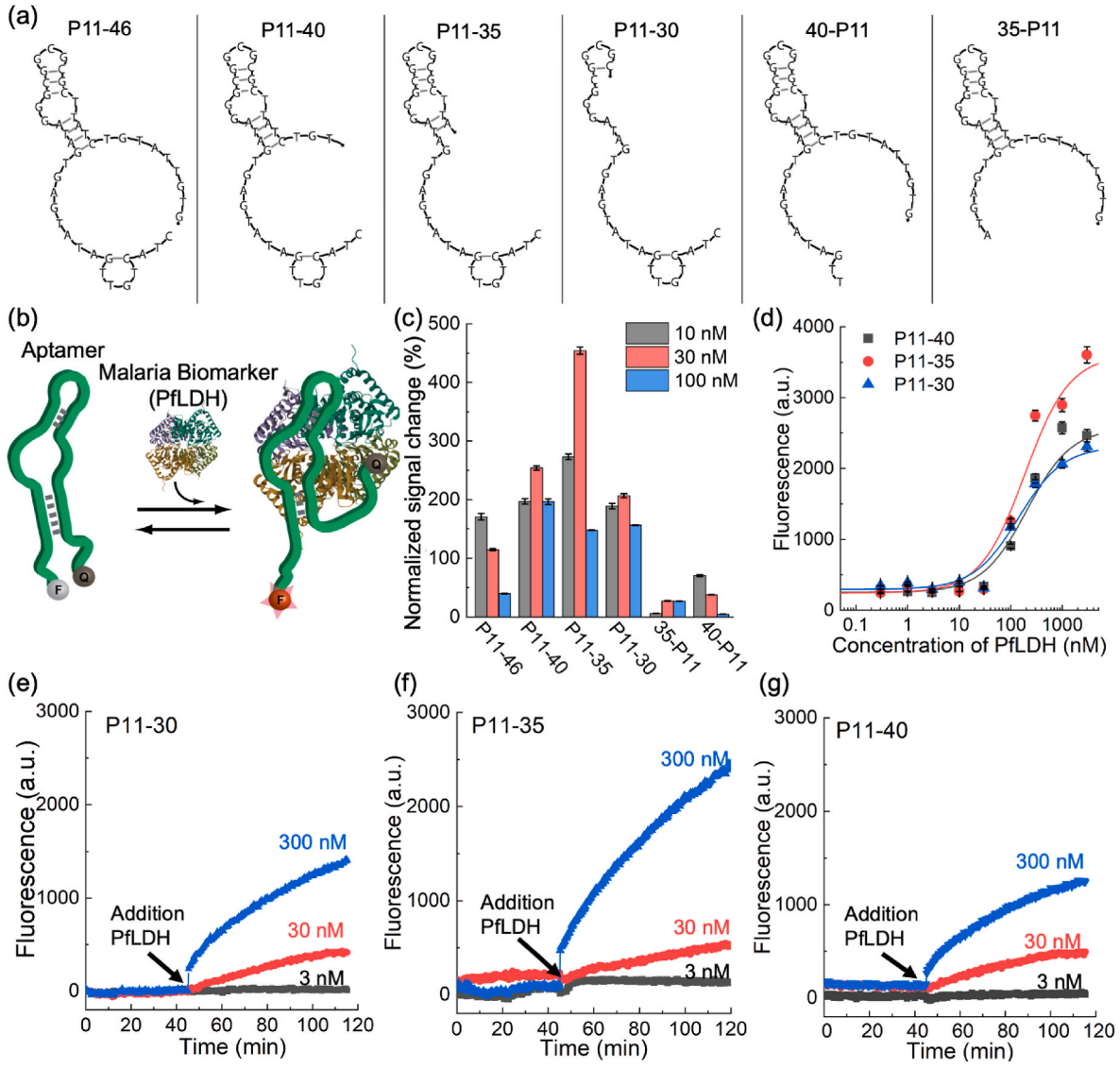

Fig. 2. Optical characterization of the re-engineered aptamer variants. (a) We truncated the aptamer sequence of P11-46 in order to maximize the binding-induced conformational change. We have renamed those sequences using the parent's name, the total number of bases and the side of the truncation. For example, the aptamer called 2008-30 indicates the 2008 aptamer which has 5 bases removed from its 3′ end, making it 30 bases long (the full list of aptamer sequences is reported in Supporting Info Table S1). During the truncation process, to do not affect the binding properties of the newly aptamer variants, we maintained the putative binding pocket constant (Fig. 1 SI). Of note, to better visualize the asymmetric truncation process we represent the different variants using the native conformation of the parent aptamer. (b) In order to assess the ability of the aptamers to undergo a binding-induced conformational change we modified them with a fluorophore and a quencher pair. In this way in the presence or absence of the target the distance between the fluorophore and quencher should differ and that generates a measurable fluorescent signal. (c) Preliminary screening testing the optical probes (each one at three different concentrations: 10, 30 and 100 nM) with a blank or with 300 nM of PfLDH. (d) The three most promising variants were further characterized performing a saturation binding curve between 300 pM and 3 μM PfLDH. (e–g) Finally, we tested the binding kinetics of the three most promising variants (P11-30, P11-35 and P11-40) upon the addition of 3, 30 and 300 nM.

with a fluorophore/quencher pair. Specifically, we modified their sequence at the 5′ end with a fluorophore (6-fam) and at the 3′ end with a quencher (BMN-Q535). When the PfLDH is added to the solution, only those variants that recognize the target through a binding-induced conformational change will be able to change the distance between the fluorophore and the quencher, generating a measurable change in fluorescent signal (Fig. 2B). We tested three different aptamer concentrations (10, 30, and 100 nM) against the absence or in the presence of a high concentration of PfLDH (300 nM) (Fig. 2C). The 2008 aptamer variants produce a small normalized signal change (less than 50% in all cases) demonstrating the failure of the re-engineering process and their inability to undergo binding-induced conformational change (Fig. S4). In contrast, P11 variants are more responsive to the addition of PfLDH (Fig. 2C). For example, 30 nM of the P11-35 variant almost produced a +500% normalized signal change, and the P11-40 and P11-30 variants produced signal changes of +200%. Based on these results we selected these three variants (P11-40, P11-35, P11-30) showing the highest fluorescent signal change. In addition, we note that the truncation of the parent aptamer at 3' end do not lead to responsive variants. It is important to note that these results do not question the ability of the aptamers to bind target, but rather their ability to undergo a binding-induced conformational change; as shown by its successful use in impedimetric (Figueroa-Miranda et al., 2018, 2020) and plasmonic (Minopoli et al., 2020) sensors.

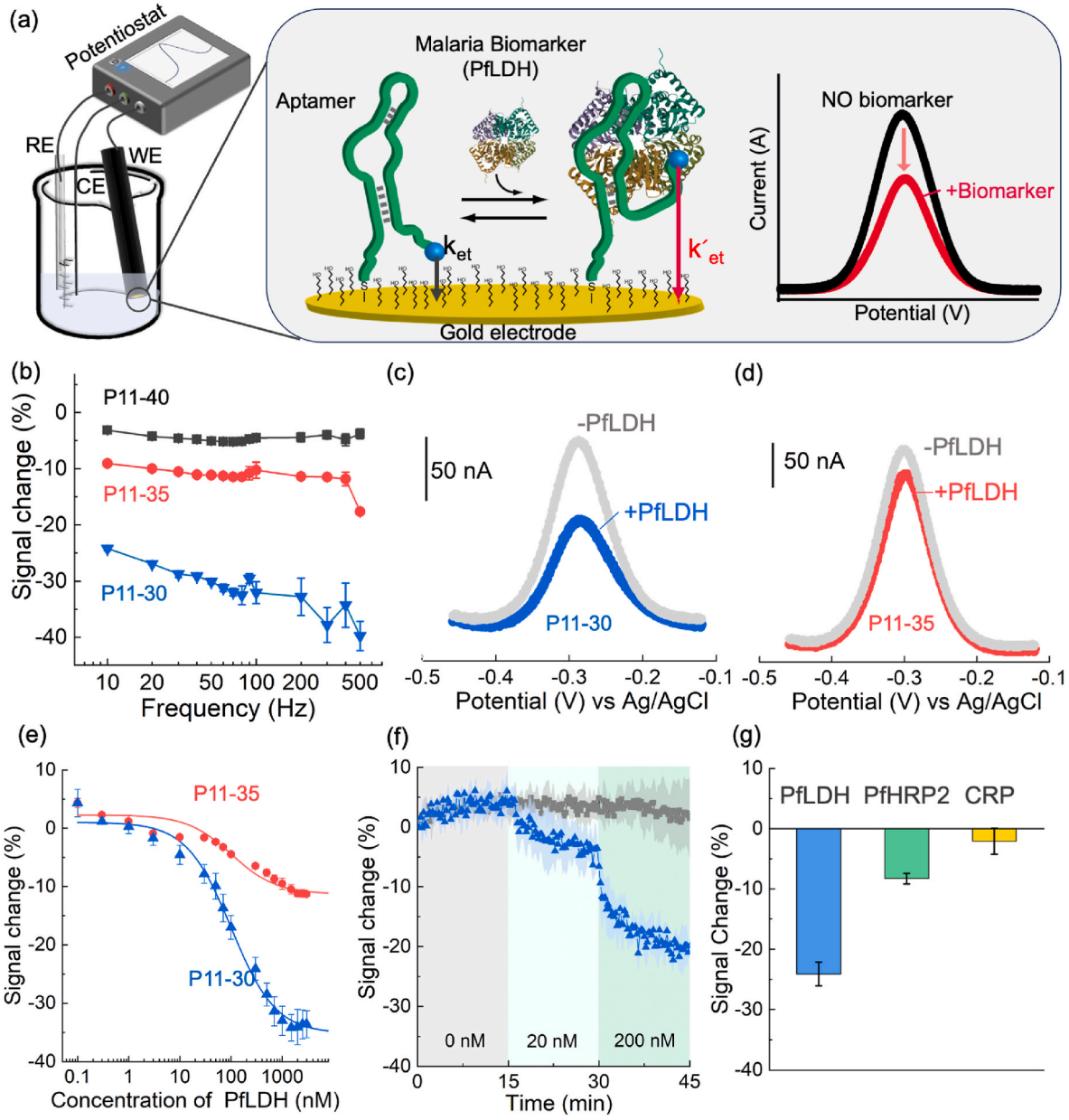

Fig. 3. Electrochemical optimization and characterization. (a) Cartoon of the experimental set-up used to characterize the aptamer variants and EAB sensor signal-transduction mechanism. (b) We challenged the three different EAB sensors with a saturating concentration of PfLDH (900 nM) and tested fourteen different frequencies. The EAB sensor based on P11-40 was unable to distinguish between the different PfLDH concentrations and was discarded. (c–d) Representative square wave voltammograms collected in the absence (gray) and in the presence of the target (colored), for the P11-30 and P11-35 variants (e) We then performed the saturation binding curves using P11-35 and P11-30 covering the whole PfLDH clinical range. The results show how P11-30 was providing the higher signal change of approximately −36% in comparison to P11-35 with only approximately −11%. (f) The kinetic measurements using P11-30 show both its stability in PBS and its responsive behaviour to the addition of PfLDH showing a response time in the order of few minutes. Finally, (g) we tested the EAB sensors against 300 nM of HRP2 and CRP, showing that the sensor is specific for PfLDH.

Next, we characterized the binding activity of the selected re-engineered aptamers. To do this, we performed saturation binding curves by challenging each of the three variants with increasing concentrations of PfLDH from 300 pM to 3 μM (Fig. 2D). Fitting the collected data using a Langmuir isotherm equation (see the Materials and Methods section), we estimated the dissociation constant values (K_d) of the variants for the protein target. We find that the K_d values for the variants P11-40, P11-35, and P11-30 are 212 ± 59 nM, 197 ± 64 nM, and 161 ± 47 nM, respectively. From the K_d values, we observe that the aptamer variants display similar affinities and the re-engineering process did not affect the binding efficiency. The obtained K_d values are comparable with the K_d value estimated for the parent aptamer (Frith et al., 2018). Examining the maximum signal-to-noise ratio, P11-35 provides the highest value of 1420%, suggesting it has the largest binding-induced conformational change. In contrast, the P11-40 sequence showed the lowest signal change, which is expected given its longer sequence and more stable structure (Fig. S5).

Finally, we characterized the binding kinetics of the variants P11-40, P11-35, and P11-30. After we achieved a stable baseline for each variant (30 nM), we challenged them with three different concentrations of target (3, 30, and 300 nM) and we collected the fluorescent signal over time (Fig. 2E–G). Supporting the previous data, the variant P11-35 provided the highest signal when challenged with 300 nM of PfLDH, almost two times higher than the signals obtained by P11-30 and P11-40. Fitting the kinetic data with a single exponential decay equation, we observe that P11-35 has the smallest equilibration time constant of 2.5 min, and, P11-30 and P11-40 have a bit higher time of 9.3 min and 11.4 min, respectively. Therefore, the aptamer variants do not only display affinity in the clinically relevant range but also are rapid enough to support point-of-care applications. To this purpose, we replaced the fluorophore and the quencher with a thiol group at 5-ends and AttoMB2 (a methylene blue derivative) at 3-ends as a redox tag for the their electrochemical characterization.

3.3. Electrochemical optimization and characterization

The EAB sensors fabricated using the re-engineered aptamer variants respond to the presence of the target PfLDH when interrogated by square-wave voltammetry (SWV) (Fig. 3). To obtain the optimal electrochemical response of EAB sensors, we characterized the effect of the SWV potential frequencies on the magnitude and sign of the signal change upon target binding (Fig. 3B). White and Plaxco (2010) To perform such an optimization, we challenged P11-30, P11-35, and P11-40 with a saturating concentration of PfLDH (900 nM), and we measured the frequency response of the sensors over SWV frequencies ranging from 10 to 500 Hz (Fig. 3B–D). All the sensors display a negative signal change. In particular, we find that P11-30 and P11-35 show the highest signal change upon the addition of PfLDH (Fig. 3B–D). In contrast, the P11-40 variant produces a small negative signal change suggesting that the conformational change is smaller in the presence of the target. These observations are consistent with previous findings showing that longer aptamers, when used in EAB sensors, tend to produce lower signal changes (Shaver et al., 2022; Wang et al., 2020). We believe that this is due to the fact that binding to the target does not affect the methylene blue moiety as much as it does for shorter aptamers. For this reason, we then continued the electrochemical characterization with just P11-30 and P11-35 variants.

The P11-30 and P11-35 sensors provide a sensitive tool for measuring PfLDH in the nanomolar range. We performed two saturation binding curves challenging P11-30 and P11-35 with increasing concentrations of PfLDH covering the entirety of the clinical range, 6.28–51.7 nM (Fig. 3E). Plucinski et al. (2019) Both EAB sensors responded to the addition of the target and the signals obtained could be fitted to a Langmuir equation, from which we could estimate the following values: P11-30 generated a K_d of 136 ± 17 nM (the confidence intervals reported here reflect standard deviations, to illustrate sensor-to-sensor variability, derived using at least three independently fabricated sensors), a dynamic range (the interval of concentrations whose signal corresponds to 10% and 90% of the maximum response) of 18.7–1200 nM, and a maximum signal change of 36%; whereas P11-35 generated a K_d of 267 ± 130 nM, a dynamic range of 16–3800 nM and a maximum signal change of 11%. Considering that P11-30 had the strongest signal change and the lower K_d, we decided to use for the development of our EAB sensor.

The developed EAB sensor is rapid and highly specific to fully support point-of-care measurement. We measured the voltammetric signal over time in the absence and presence of 20 nM and 200 nM PfLDH added respectively after 15 and 30 min (Fig. 3F). The kinetic measurements show that the EAB sensor provides a stable baseline in the absence of the target (only PBS) while the presence of PfLDH induce a signal change describing a exponential decay of the signal, as expected. Again, the equilibration time constants estimated (3.5 min) demonstrate that the sensor is rapid to support point-of-care platform. Finally, we challenged the EAB sensor with interference molecules to test its specificity. Specifically, we challenged it with 300 nM of the protein HRP2 (as we seen in the introduction another malaria biomarker) and the C-Reactive Protein (CRP, a common inflammatory biomarker) (Fig. 3G). In the case of HRP2 we observe a signal change of approximately 8% and for CRP of approximately 2% which are respectively 3 and 12 times lower than the signal obtained using PfLDH. To ensure the specificity of the EAB sensor, we tested it with an alternative DNA sequence. This sequence, previously reported as an aptamer specific for another P. falciparum biomarker (HRP2), was challenged with 300 nM PfLDH (Lo et al., 2021). Its minimal signal change of 0.07% ± 0.8% demonstrates the specificity of the developed EAB sensor (Fig. S6).

3.4. Measurements in human blood

Our EAB sensor is selective to perform measurements directly in complex matrices. To demonstrate this, we firstly assessed the stability of the sensor in diluted human blood (Fig. 4A). To do this, we placed the sensor in 1% diluted whole blood (in PBS solution) and we collected the signal over time. We find that our EAB sensor is stable within the time required for point-of-care measurement: the signal change only exhibited the fluctuation of approximately 2% within 15 min (Fig. 4B). Afterwards, the signal still kept stable for additional 25 min, and then we observed a stable drift due to the non-specific adsorption of blood cells, proteins and other blood components on the electrode surface (Fig. S7). This drift in blood has been previously reported for other EAB sensors (Arroyo-Currás et al., 2020). We then characterized the ability of our device to measure PfLDH in human blood and performed a saturation binding curve in 1% diluted whole blood (Fig. 4C). The resulting binding curve produce a signal change of −17% with a K_d of 27.9 ± 4.4 nM and a dynamic range of 3.8–205.7 nM (Fig. 4C). These results indicate that indeed the P11-30 aptamer has the ability to bind to PfLDH in diluted blood. The corresponding voltammograms intuitively demonstrate the reduction of the current peak with the addition of PfLDH from 0 to 700 nM (Fig. 4D). To further evaluate the accuracy of the P11-30 sensor in diluted blood, six electrodes were fabricated under identical conditions and tested with 10 nM PfLDH spiked into 1% blood. The signal changes from these electrodes closely matched the calibrated value (red dashed line) (Fig. 4E). The calibrated concentration derived from the results of these six electrodes was 10.06 ± 1.52 nM, indicating good accuracy.

As briefly mentioned in the introduction, current gold-standard malaria diagnostic techniques predominantly rely on laboratory-based methods, such as microscopy and PCR, and in some cases on multi-step immunological approaches like ELISA. While these methods typically provide sensitive and quantitative results, they require expensive equipment and trained personnel, limiting their use in point-of-care settings. In contrast, lateral flow assays (LFAs) are widely employed in low-resource areas because they are user-friendly and cost-effective. However, LFA results are primarily qualitative, and faint test lines

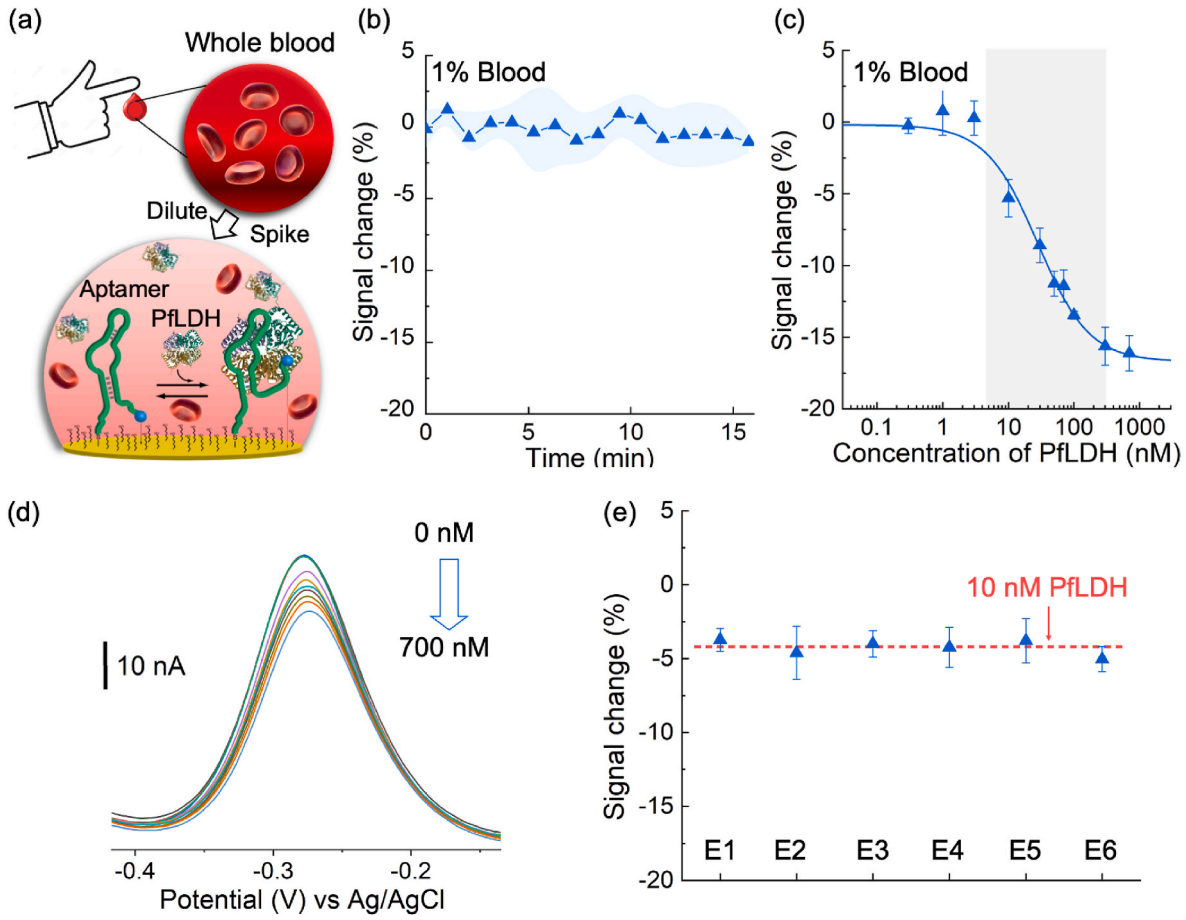

Fig. 4. Applicability of the EAB sensor in diluted blood. (b)The stability of EAB sensor in 1% of human blood (in PBS) was tested. (c) We assessed the signal change of EAB sensor in 1% of human blood (in PBS), showing a typical sigmoidal curve with increasing concentration of PfLDH. (d) The corresponding voltammograms. From top to bottom, EAB sensor detect 0–700 nM PfLDH. (e) The signal change of 6 electrodes to 10 nM PfLDH in 1% of human blood in PBS. The error bar represents the three measurement by one electrode. Red dashed line highlights the signal change to 10 nM PfLDH from the binding curve. (For interpretation of the references to color in this figure legend, the reader is referred to the Web version of this article.)

may lead to subjective interpretation and reduced accuracy. To address these challenges, EAB sensors offer a quantitative readout comparable to laboratory-based tests while being at least as user-friendly as LFAs—if not more so. Table S2 provides a more detailed comparison of the different methods.

4. Conclusions

In this work we presented the fabrication and characterization of a novel EAB sensor for the convenient and rapid measurement of the malaria biomarker PfLDH. We successfully re-engineered the PfLDH-binding P11 aptamer to undergo a binding-induced conformational change and to be adapted as bioreceptor in the EAB sensing platform. Using fluorescence spectroscopy we characterized the different aptamer variants generated from the rational design of the parent aptamer sequence. The optical characterization allowed us to progressively shortlist the most promising aptamers until identifying the P11-40, P11-35 and P11-30 variants as the best candidates. Then, we tested them on the electrochemical platform and we demonstrate their ability to produce responsive EAB sensors. We selected the P11-30 variant for the best analytical performance demonstrating its ability to rapidly detect the target in the nanomolar range with high specificity. Finally, we provided a demonstration of our EAB sensor ability to measure PfLDH in diluted human blood providing a new tool for the diagnosis of malaria.

Although we could not find an official concentration range for PfLDH in blood, in the 2019 work by Plucinski et al. the authors analyzed 196 uncomplicated malaria in Angolan children and found that the concentration of PfLDH ranged from 6.28 nM to 51.7 nM (Plucinski et al., 2019). Considering that in high parasitemia and severe malaria cases, particularly in high-prevalence regions, the level of PfLDH can be significantly elevated. In some reported cases, the concentration has been observed to reach as high as 600 nM. (Carme and Demar, 2013; Omingo, 2024). Therefore, the developed EAB sensor can partially cover the clinical range of PfLDH missing the lower nanomolar concentrations. To improve the sensitivity, the parent aptamer sequence could be selected with new SELEX techniques (Wen et al., 2023), which could couple high affinity with a large-scale conformational change. In fact, to the best of our knowledge, this is the first EAB sensor for PfLDH that do not require the subsequent addition of redox species and it complements the work published by Prof. Tanner's group on an EAB sensor for HRP2 (Lo et al., 2021). We believe these results highlight the potential of EAB sensors to provide quantitative results akin to laboratory-based assays, while maintaining the user-friendliness of LFA. Overall, these results pave the way for further exploration of EAB sensors in practical applications, bridging the gap between academic research and clinical practice.

CRediT authorship contribution statement

Qiuyue Yang: Writing – review & editing, Writing – original draft, Methodology, Investigation, Formal analysis, Data curation, Conceptualization. **Julia Pedreira-Rincón:** Writing – review & editing,

Resources, Project administration, Methodology. **Leire Balerdi-Sarasola:** Writing – review & editing, Supervision, Resources, Methodology, Investigation, Funding acquisition, Conceptualization. **Luis Baptista-Pires:** Writing – review & editing, Resources, Project administration, Investigation, Funding acquisition, Conceptualization. **Jose Muñoz:** Writing – review & editing, Supervision, Resources, Project administration, Methodology, Investigation, Funding acquisition, Conceptualization. **Daniel Camprubí-Ferrer:** Writing – review & editing, Supervision, Resources, Methodology, Investigation, Funding acquisition, Conceptualization. **Andrea Idili:** Writing – review & editing, Visualization, Supervision, Methodology, Investigation, Data curation, Conceptualization. **Claudio Parolo:** Writing – review & editing, Writing – original draft, Supervision, Resources, Project administration, Methodology, Investigation, Funding acquisition, Conceptualization.

Declaration of competing interest

The authors declare that they have no conflicts of interest related to the content of this manuscript.

Acknowledgment

The ISGlobal authors acknowledge support from the Spanish Ministry of Science and Innovation and State Research Agency through the "Centro de Excelencia Severo Ochoa 2019–2023" Program (CEX2023-0001290-S), CIBER-Consorcio Centro de Investigación Biomédica en Red-(CB21/13/00112), Instituto de Salud Carlos III, Spanish Ministry of Science and Innovation and European Union, and support from the Generalitat de Catalunya through the CERCA Program and AGAUR programme (2021 SGR 01558). They also acknowledge support from the Spanish Ministry of Science and Innovation through the program PID2020-116770RJ-I00 and CPP2021-008658. C.P. acknowledges support from the Hospital Clinic of Barcelona, the CaixaResearch Institute Innovation Hub and from the Spanish Ministry of Science through the Ramón y Cajal grant no. RYC2022-036743-I. J.P.R. acknowledges the predoctoral program AGAUR-FI ajuts (2024 FI-3 00065) Joan Oró de la Secretaria d'Universitats i Recerca del Departament de Recerca and Universitats de la Generalitat de Catalunya i del Fons Europreu Social. L. B.P. acknowledges FCT I.P. for the research action 2021.04477.CEECIND and the financial support within the scope of the project i3N, UIDB/50025/2020 & UIDP/50025/2020, LA/P/0037/2020, financed by national funds through the FCT/MEC.

We also thank all CEK "support" team and in particular Cristina Canaleta, Laura Muñoz, Laura Puyol, Diana Barrios and the other research groups from ISGlobal and IDIBAPS. We particularly thank Maria Ribera Ruché and Miriam Ramirez from the Nanomalaria group for their technical support. We also thank all the healthcare personnel of the Travel Medicine Clinic of the Hospital Clinic of Barcelona.

Appendix A. Supplementary data

Supplementary data to this article can be found online at https://doi.org/10.1016/j.bios.2025.117152.

Data availability

Data will be made available on request.

References

Arroyo-Currás, N., Dauphin-Ducharme, P., Scida, K., Chávez, J.L., 2020. From the beaker to the body: translational challenges for electrochemical, aptamer-based sensors. Anal. Methods 12, 1288–1310. https://doi.org/10.1039/D0AY00026D.

Arroyo-Currás, N., Somerson, J., Vieira, P.A., Ploense, K.L., Kippin, T.E., Plaxco, K.W., 2017. Real-time measurement of small molecules directly in awake, ambulatory animals. Proc. Natl. Acad. Sci. 114, 645–650. https://doi.org/10.1073/pnas.1613458114.

Balanza, N., Erice, C., Ngai, M., Varo, R., Kain, K.C., Bassat, Q., 2020. Host-based prognostic biomarkers to improve Risk stratification and outcome of febrile children in low- and middle-income countries. Front. Pediatr. 8, 552083. https://doi.org/10.3389/fped.2020.552083.

Balerdi-Sarasola, L., Parolo, C., Fleitas, P., Cruz, A., Subirà, C., Rodríguez-Valero, N., Almuedo-Riera, A., Letona, L., Álvarez-Martínez, M.J., Valls, M.E., Vera, I., Mayor, A., Muñoz, J., Camprubí-Ferrer, D., 2023. Host biomarkers for early identification of severe imported Plasmodium falciparum malaria. Travel Med. Infect. Dis. 54, 102608. https://doi.org/10.1016/j.tmaid.2023.102608.

Ballard, E., Wang, C.Y.T., Hien, T.T., Tong, N.T., Marquart, L., Pava, Z., Tarning, J., O'Rourke, P., McCarthy, J.S., 2019. A validation study of microscopy versus quantitative PCR for measuring Plasmodium falciparum parasitemia. Trop. Med. Health 47, 49. https://doi.org/10.1186/s41182-019-0176-3.

Bell, D., Visser, T., 2016. Malaria Diagnostic Platform: Lateral Flow Assays, Encyclopedia of Malaria. Springer, New York, NY. https://doi.org/10.1007/978-1-4614-8757-9_105-1.

Bourzac, K., 2014. Infectious disease: beating the big three. Nature 507, S4–S7. https://doi.org/10.1038/507S4a.

Carme, B., Demar, M., 2013. Hyperparasitaemia during bouts of malaria in French Guiana. Malar. J. 12, 20. https://doi.org/10.1186/1475-2875-12-20.

Cheung, Y.-W., Kwok, J., Law, A.W.L., Watt, R.M., Kotaka, M., Tanner, J.A., 2013. Structural basis for discriminatory recognition of Plasmodium lactate dehydrogenase by a DNA aptamer. Proc. Natl. Acad. Sci. 110, 15967–15972. https://doi.org/10.1073/pnas.1309538110.

Curtis, S.D., Ploense, K.L., Kurnik, M., Ortega, G., Parolo, C., Kippin, T.E., Plaxco, K.W., Arroyo-Currás, N., 2019. Open source software for the real-time control, processing, and visualization of high-volume electrochemical data. Anal. Chem. 91, 12321–12328. https://doi.org/10.1021/acs.analchem.9b02553.

Figueroa-Miranda, G., Feng, L., Shiu, S.C.C., Dirkzwager, R.M., Cheung, Y.W., Tanner, J. A., Schöning, M.J., Offenhäusser, A., Mayer, D., 2018. Aptamer-based electrochemical biosensor for highly sensitive and selective malaria detection with adjustable dynamic response range and reusability. Sensors Actuators B Chem 255, 235–243. https://doi.org/10.1016/J.SNB.2017.07.117.

Figueroa-Miranda, G., Wu, C., Zhang, Y., Nörbel, L., Lo, Y., Tanner, J.A., Elling, L., Offenhäusser, A., Mayer, D., 2020. Polyethylene glycol-mediated blocking and monolayer morphology of an electrochemical aptasensor for malaria biomarker detection in human serum. Bioelectrochemistry 136, 107589. https://doi.org/10.1016/j.bioelechem.2020.107589.

Frith, K.A., Fogel, R., Goldring, J.P.D., Krause, R.G.E., Khati, M., Hoppe, H., Cromhout, M.E., Jiwaji, M., Limson, J.L., 2018. Towards development of aptamers that specifically bind to lactate dehydrogenase of Plasmodium falciparum through epitopic targeting. Malar. J. 17, 191. https://doi.org/10.1186/S12936-018-2336-Z.

Global Malaria Programme, 2023. WHO.

Global Tecnichal Strategy for Malaria, 2021. Geneve.

Hendriksen, I.C.E., Mwanga-Amumpaire, J., von Seidlein, L., Mtove, G., White, L.J., Olaosebikan, R., Lee, S.J., Tshefu, A.K., Woodrow, C., Amos, B., Karema, C., Saiwaew, S., Maitland, K., Gomes, E., Pan-Ngum, W., Gesase, S., Silamut, K., Reyburn, H., Joseph, S., Chotivanich, K., Fanello, C.I., Day, N.P.J., White, N.J., Dondorp, A.M., 2012. Diagnosing severe falciparum malaria in parasitaemic African children: a prospective evaluation of plasma PfHRP2 measurement. PLoS Med. 9, e1001297. https://doi.org/10.1371/JOURNAL.PMED.1001297.

Home - MESA, 2011. WWW Document]. URL. https://mesamalaria.org/.

Idili, A., Parolo, C., Alvarez-Diduk, R., Merkoçi, A., 2021. Rapid and efficient detection of the SARS-CoV-2 spike protein using an electrochemical aptamer-based sensor. ACS Sens. 6, 3093–3101. https://doi.org/10.1021/ACSSENSORS.1C01222/.

Lo, Y., Cheung, Y.W., Wang, L., Lee, M., Figueroa-Miranda, G., Liang, S., Mayer, D., Tanner, J.A., 2021. An electrochemical aptamer-based biosensor targeting Plasmodium falciparum histidine-rich protein II for malaria diagnosis. Biosens. Bioelectron. 192, 113472. https://doi.org/10.1016/J.BIOS.2021.113472.

Lynch, E., Jensen, T.O., Assao, B., Chihana, M., Turuho, T., Nyehangane, D., Manyok, J. B., Pasquale, H., Khim, N., Witkowski, B., Coldiron, M.E., 2022. Evaluation of HRP2 and pLDH-based rapid diagnostic tests for malaria and prevalence of pfhrp2/3 deletions in Aweil, South Sudan. Malar. J. 21, 261. https://doi.org/10.1186/S12936-022-04280-W.

Malaria Vaccine: WHO Position Paper – May 2024, 2024.

Minopoli, A., Della Ventura, B., Lenyk, B., Gentile, F., Tanner, J.A., Offenhäusser, A., Mayer, D., Velotta, R., 2020. Ultrasensitive antibody-aptamer plasmonic biosensor for malaria biomarker detection in whole blood. Nat. Commun. 111 11, 1–10. https://doi.org/10.1038/s41467-020-19755-0, 2020.

NUPACK-Cloudalpha, 2006. WWW Document]. URL. https://www.nupack.org/.

Omingo, R.A., 2024. Histidine Rich Protein Ii and Lactate Dehydrogenase Levels in Saliva and Blood in Acute Malaria Cases in Kisumu, Western kenya. Maseno Univ.

Parolo, C., Idili, A., Heikenfeld, J., Plaxco, K.W., 2023. Conformational-switch biosensors as novel tools to support continuous, real-time molecular monitoring in lab-on-a-chip devices. Lab Chip 23, 1339–1348. https://doi.org/10.1039/D2LC00716A.

Parolo, C., Idili, A., Ortega, G., Csordas, A., Hsu, A., Arroyo-Currás, N., Yang, Q., Ferguson, B.S., Wang, J., Plaxco, K.W., 2020a. Real-time monitoring of a protein biomarker. ACS Sens. 5, 1877–1881. https://doi.org/10.1021/acssensors.0c01085.

Parolo, C., Sena Torralba, A., Bergua, J., Calucho, E., Fuentes Chust, C., Hu, L., Rivas, L., Álvarez Diduk, R., Nguyen, E., Cinti, S., Quesada González, D., Merkoçi, A., 2020b. Tutorial: design and fabrication of nanoparticle- based lateral-flow immunoassays. Nat. Protoc. 15, 3788–3816. https://doi.org/10.1038/s41596-020-0357-x.

Plucinski, M.M., McElroy, P.D., Dimbu, P.R., Fortes, F., Nace, D., Halsey, E.S., Rogier, E., 2019. Clearance dynamics of lactate dehydrogenase and aldolase following antimalarial treatment for Plasmodium falciparum infection. Parasit. Vectors 12, 293. https://doi.org/10.1186/s13071-019-3549-x.

Poti, K.E., Sullivan, D.J., Dondorp, A.M., Woodrow, C.J., 2020. HRP2: transforming malaria diagnosis, but with caveats. Trends Parasitol. 36, 112–126. https://doi.org/10.1016/j.pt.2019.12.004.

Shaver, A., Mahlum, J.D., Scida, K., Johnston, M.L., Aller Pellitero, M., Wu, Y., Carr, G. V., Arroyo-Currás, N., 2022. Optimization of vancomycin aptamer sequence length increases the sensitivity of electrochemical, aptamer-based sensors in vivo. ACS Sens. 7, 3895–3905. https://doi.org/10.1021/acssensors.2c01910.

Van Enter, B.J., Von Hauff, E., 2018. Challenges and perspectives in continuous glucose monitoring. Chem. Commun. 54, 5032–5045. https://doi.org/10.1039/c8cc01678j.

Wang, C., Liu, L., Zhao, Q., 2020. Low temperature greatly enhancing responses of aptamer electrochemical sensor for aflatoxin B1 using aptamer with short stem. ACS Sens. 5, 3246–3253. https://doi.org/10.1021/acssensors.0c01572.

Wen, K., Chen, Y., Meng, X., Botros, S., Dai, W., Stojanovic, M.N., Tomer, R., Lin, Q., 2023. A microfluidic dual-aptamer sandwich assay for rapid and cost-effective detection of recombinant proteins. Microchem. J. 188, 108454. https://doi.org/10.1016/j.microc.2023.108454.

White, R.J., Plaxco, K.W., 2010. Exploiting binding-induced changes in probe flexibility for the optimization of electrochemical biosensors. Anal. Chem. 82, 73–76. https://doi.org/10.1021/ac902595f.

World Malaria Report 2023, 2023. Geneve.

Xiao, Y., Lai, R.Y., Plaxco, K.W., 2007. Preparation of electrode-immobilized, redox-modified oligonucleotides for electrochemical DNA and aptamer-based sensing. Nat. Protoc. 2, 2875–2880. https://doi.org/10.1038/nprot.2007.413.